PROCEEDINGS OF SCIENCE

ARGO-YBJ absolute energy scale calibration for light primaries in the multi TeV region by using the moon shadow

Min Zha, LingLing Ma for the ARGO-YBJ Collaboration
IHEP
E-mail: zham@ihep.ac.cn

On the base of its high altitude and nearly full coverage, the ARGO-YBJ experiment could play a important role in bridging satellite/balloon-borne and indirect measurement in the energy spectrum measurment. In this work the light component (proton + helium like) of cosmic rays can be selected from the shower lateral information and the energy of the cosmic ray light component will be calculated. Combining the westward displacement of moon shadow position direction using the same set of data, the construction of an energy scaler from air shower experiment is discussed.

The 34th International Cosmic Ray Conference,
30 July- 6 August, 2015
The Hague, The Netherlands

PoS(ICRC2015)344

1. Introduction

Energy calibration is a difficult question in air shower array experiments. For a long time the normalization or reference of the energy measurements using air shower array detection technique, is offered from the direct measurements using a satellite or a balloon-borned detector due to their well calorimeters and charge sensitive detectors. It is also worth to note that typically the calorimeter of satellite or balloon-borned detectors has been well calibrated using the accelerator beam up to few hundreds of GeV, not in TeV energy region which is more interested for high altitude air shower experiments. In this work, we report another idea about energy calibration in indirect, ground-based air shower arrays using moon shadow at TeV energies. The so-called moon shadow is firstly raised by Clark in 1957[2]. This effect has been observed by many different experiments, including typical air showers and neutrino experiment and muon detectors[3, 4, 5]. As the position of the cosmic-ray Moon shadow depends upon the paths of the particles through the geomagnetic field, particles with a lower magnetic rigidity will be deflected more than particles of a higher rigidity. Roughly speaking the deflected angle in the east-west direction can be approximated as $\Delta\theta \approx \frac{1.6^\circ}{E(TeV)/Z}$ in a word the Earth-Moon system can be considered as a spectrometer. Based on this aspect, paper [3, 6] have proceed some works about absolute rigidity scale calibration without cosmic ray primary composition discrimination.

Recently with many progresses achieved in cosmic ray elemental energy spectrum observed by ATIC-2, CREAM and PAMELA [7, 8, 9, 10] and the update of high energy hadronic interaction models with the LHC data and the lower of the threshold energy of ground-based air shower arrays, further progress can be achieved. ARGO-YBJ experiment is a good candidate, because of its high altitude observation, its full coverage detector and good angular resolution, the deflected moon shadow data induced by cosmic ray light showers (proton+helium-like) could be clearly measured, a direct link between shower size and primary energy could be established using these light moon shadow data. And as an examination for this calibrated energy, the primary proton+helium energy spectrum using the same light moon shadow data in the energy between 3 TeV to 50 TeV is measured event by event. Through these measurements a calibrated energy scale and energy resolution is constructed.

2. The ARGO-YBJ Detector

The ARGO-YBJ detector is located at the Yang-Ba-Jing Cosmic Ray Observatory (Tibet, China, 30.11°N, 90.53°E) at an altitude of 4300 m a.s.l., corresponding to a vertical atmospheric depth of 606 g/cm^2. It consists of a single layer of Resistive Place Chambers (RPCs), with each RPC (2.8×1.25 m^2) divided into 10 basic detection units called pads (55.6×61.8 cm^2). Each pad consists of 8 digital readout strips. Twelve RPCs are grouped into a cluster (5.7×7.6 m^2). The central carpet (78×74 m^2) of the detector is fully covered by 130 clusters, whereas 23 clusters form a guard ring surrounding the central carpet for a better shower core reconstruction. The whole array covers a total area of about $11,000$ m^2. To extend the dynamic range, a charge read-out layer has been implemented by instrumenting each RPC with two large-size pads called "big-pad" (140×122.5 cm^2 each) [11]. Two independent DAQ systems are implemented in the detector: the scaler mode and the shower mode. In current work, only the data from the shower mode are used.

In this mode, the arrival time and fired strip pattern of each fired pad are recorded for subsequent geometric reconstruction. The trigger threshold refers to the number of fired pads greater than 20 within the 420 ns triggering window, whereas average trigger rate is about 3.5 kHz [12]. The completed ARGO-YBJ detector has been collecting data since November 2007 and end its data taking on Feb. 2013.

For triggered events, the shower core position was reconstructed with the fitting of lateral distribution of fired signal with a modified Nisimura-Kamata-Greisen-like function. The arrival direction of each shower was estimated by fitting the shower front with a planar fitting and a further correction on the curvature of the showers, the slope of this conical shape is fixed to 0.03 ns/m. Based on the simulation, the resolution of shower core is better than 7 meter and the angular resolution is better than 0.8 degree as number of fired strips is higher than 400, $N_{strips} \geq 400$.

3. Monte Carlo Simulation and Data Selection

3.1 Monte Carlo simulation

An extensive Monte Carlo simulation were carried out to consider geomagnetic field, the air shower cascade development in the atmosphere and the response in the ARGO-YBJ detector. For the geomagnetic field, International Geomagnetic Reference Field 11th(IGRF11) [13] generation model was used to describe the earth's field. Air showers were simulated in the CORSIKA-v7350 package [14]. The low and high energy hadronic models used were Fluka [15] and EPOS-LHC [16] respectively. All shower secondary particles have been traced down to the energy threshold of 30 MeV for hadrons and muons and 1 MeV for electron-magnetic particles. Five primary types(abbreviated as H(proton), He(helium), CNO, MgAlSi and Iron groups) were simulated to treat primary chemical composition. The power index and absolute flux of single primary elements energy spectrum is set as the measurements from CREAM experiment [8, 9]. Considering about the detector trigger efficiency, the energy range of the incident cosmic ray was from 300 GeV to 1000 TeV for proton and helium, and for the rest 3 groups the energy range was from 1 TeV to 1000 PeV relatively. The incident zenith angles of primary particles were sampled along the Moon's orbit with $10^\circ \times 10^\circ$ around the Moon's center, and the maximum zenith angle were 40°. In order to improve simulation efficiency, a back-tracing method was applied, the charge of the incident primary cosmic ray was reversed and tracked it backward towards the Moon, if the primary cosmic ray was hit the Moon, it became our "moon shadow events".

The named G4argo [17] software based on GEANT4 package was used to simulate the detector response. And in this simulation, the detector performances, such as trigger logic, time resolution, electronic noises, relation between strip and pad multiplicities based on the experimental data, have been taken into account. To increase the statistics each simulated air shower event which reaches the detector observation level, the simulated air showers are re-sampled 10 times and the shower core location is randomly sampled within an area of 1500×1500 m^2 around the detector center.

3.2 light component showers selection

In this analysis, the experiment data collected from 2008 to 2012 were used. Besides later composition cuts, to keep enough statistics in estimation the moon shadow and its position, to

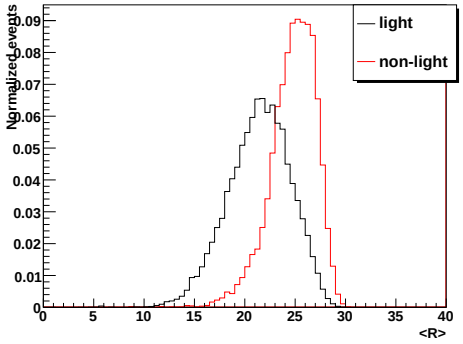

Figure 1: The distribution of the composition sensitive parameter, <R>, light is for (p+he) and non-light is from (CNO+MgAlSi+Iron) group. All cuts from section 3.2 are applied.

minimize the attenuation effect on shower size due to large inclined showers, and at the same time to select good reconstruction quality data the following cuts were applied to the simulated samples and the experimental data: (1) the shower must have $N_{strips} \geq 400$, here N_{strips} is the number of fired strips; (2) the zenith angle of selected event is less than 35 degree; (3) the shower core is located inside the area of $62 \times 62\ m^2$ around the detector center.

Cosmic rays detected by ARGO are mainly composed of protons and helium nuclei. However in order to decrease the uncertainty due to non-light species contribution, a carefully primary composition selection is adopted based on the simulation. Comparing with iron showers, for a given energy, proton or light nuclei penetrates deeper into the atmosphere, one would expect that the proton or light nuclei induced showers show up a steeper and more narrower lateral distribution. A variable, $< R >$, is calculated to select light component showers on the base of this aspect [18], $< R >$ is called as mean lateral radius, it is calculated as $< R >= \frac{\sum(N_i R_i)}{\sum N_i}$, N_i is the number of strips recorded by the i^{th} fired pad, R_i is the distance from this pad to the shower core. Fig.1 shows the distribution of the variable, here the 5 kinds of cosmic ray components are divided into light (p+he) and non-light (CNO+MgAlSi+Iron) group. The simulation results show that by requiring $< R >$ less than 24, the non-light CR contribution could be decreased to 2% as energy is higher than 1 TeV. And this ratio is around 25% if no any component selection was applied for the data samples.

4. analysis the displacement of moon shadow in east-west direction

In order to extract the deficit counts coming from the direction of moon by the light component, a $10^\circ \times 10^\circ$ moon sky map is constructed with grid size of $0.1^\circ \times 0.1^\circ$. Here direct integration method [19] is used to estimate the number of background events in each grid, the source map can be made with the light component shower events falling within each grid, then significance map is obtained after applying smoothing procedure. Total five windows in the strip range of $[400-600)$, $[600-1000)$, $[1000-2000)$, $[2000-3000)$ and ≥ 3000 are analyzed, a deficit of 13.7, 15.7, 16.8, 11.4, 12.1 sigma are accumulated. Fig.2(a) is one example, it is the significance map in the highest multiplicities window. The relative deficit counts observed in the East-West direction is found by a gaussian fit, shown in Fig.2 (b)-(f). As one expected the peak position of deficit counts is shifted westward as the primary energy decreases.

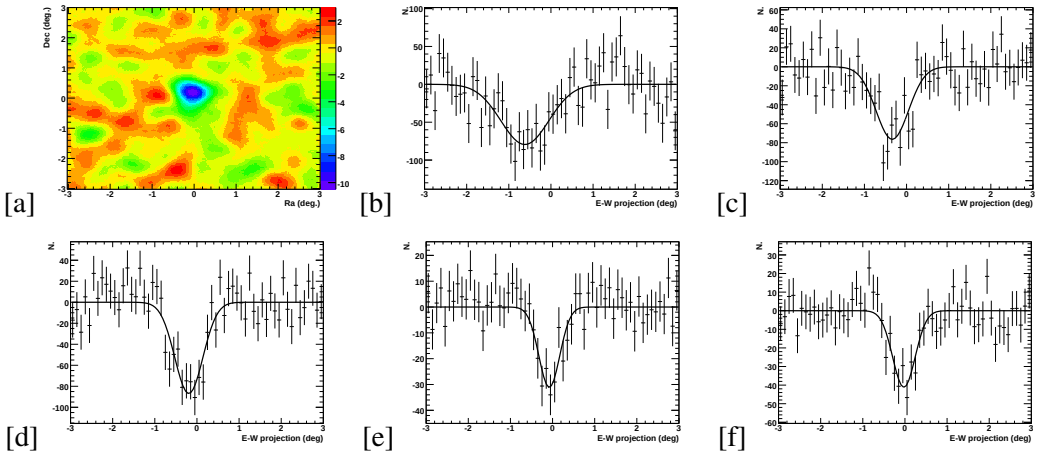

Figure 2: (a) is the significance map for selected light primary moon data at $\geq$ 3000 window, the origin of the coordinate is taken in the direction of the moon, the right-hand side color scale shows the level of the significance of the deficit in terms of the standard deviation σ. (d)-(f) are deficit counts observed around the moon projected along east-west direction in 5 observed windows, (b) $[400-600)$ (c) $[600-1000)$ (d) $[1000-2000)$ (e) $[2000-3000)$ (f) ≥ 3000

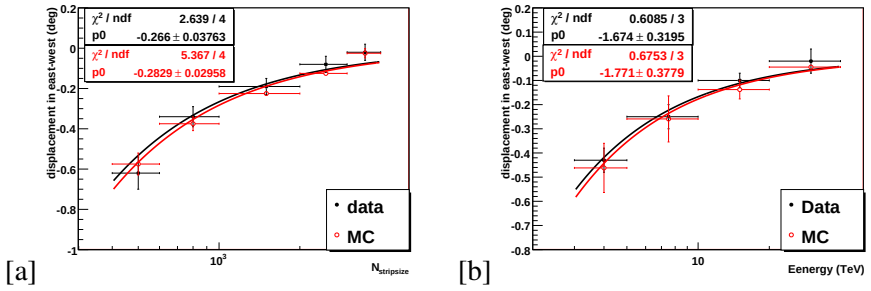

Figure 3: The Westward displacement of the moon shadow as function of N_{strips} and energy from the observed experimental data and the expected one. The error bar in X coordinate is bin width

5. Results and Discussion

5.1 Calibration primary energy

Then observed displacement of moon shadow from light component as a function of N_{strips} is shown in left panel of Fig.3 [a], few important information can be collected: (1) MC samples (red open dot) are in good agreement with data (black solid dot), both show an energy dependence as expected. If fitted the displacement with a simple linear inverse function, $P_0(N_{strips}\times 10^{-3})^{-1}$, the difference between data and MC parameter in P_0 is 6%; (2) a direct link can be constructed between N_{strips} and E_0 through simulated light moon shadow events, here the function $log10(E_0) = k+\lambda\ log10(N_{strips})$ was used to fit the distribution with k=0.81 and $\lambda = 1.00$. This gives rise to a calibration equation between N_{strips} and E_0.

As a check of this calibrated energy, we re-do light moon shadow analysis on the basis of reconstructed energy, i.e., the same observed light moon shadow data are re-analyzed in 4 windows of reconstructed energy with $[3-5)$, $[5-10)$, $[10-20)$ and $\geq$20 TeV respectively. A deficit of

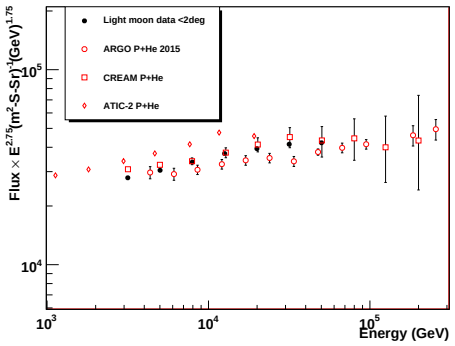

Figure 4: The differential energy spectrum of the light component measured using ARGO-YBJ light moon data compare with other measurements. The proton, helium and proton+helium from CREAM, ATIC experiment are from paper [7, 8]

13.4, 13.7, 11.8 and 10.1 sigma are accumulated. Right panel of Fig.3 shows the result, comparing with the left panel result, a 5.5% difference is existed in fitting parameters P_0. Thus we believe this reconstructed energy calibrated by using the light moon shadow data is quite a solid.

5.2 comparison on light component cosmic ray energy spectrum

To further understand this calibrated energy scale, same calibrated light moon data with opening angle less than 2 degree relative to moon center are used to calculate the differential proton+helium energy spectrum. Here differential light component spectrum is calculated according to its normal definition, $J(E) = \phi_0 E^{-\gamma} = \frac{N}{E\ A_{eff}\ \Omega\ T}$ where T is total live time, Ω is the selected solid angle relative to 2 degree; A_{eff} is the effective collection area, which can be determined from the simulation by $A_{\rm eff} = \frac{N_{\rm rec}}{N_{\rm gen}} A_{\rm gen} \frac{cos(\theta_{max})+cos(\theta_{min})}{2}$ where $N_{\rm gen}$ showers with the core position distributed over a large area $A_{\rm gen}$ and after applying same cuts as experimental data, $N_{\rm rec}$ events survives the trigger conditions, the reconstruction and other data selections cuts. And θ_{min} and θ_{max} are 0°,40° respectively. Fig.4 shows the final proton + helium spectrum between 3-50 TeV with CREAM composition assumption. Comparing with the light spectrum from ARGO-YBJ unfolding measurement and CREAM experiment, the value of the spectrum index is -2.60 ± 0.02 which agrees quite well with $\gamma_{argo-unfold} = 2.64 \pm 0.01$, $\gamma_{cream} = 2.62 \pm 0.02$. And as to the flux intensity at 50 TeV, their values are $\phi_{cream} = 5.29 \times\ 10^{-9}$, $\phi_{argo-unfold} = 4.49 \times\ 10^{-9}$ and $\phi_{moon} = 5.16 \times\ 10^{-9}$, the large difference in absolute flux is 15%. To understand such difference is still on the way, especially comparing with ARGO-unfold result, one possible reason could be the existence of no-light component contamination, at this moment the heavy component contribution has not been subtracted yet.

5.3 Systematic uncertainties

Three sources about the systematic uncertainties using this Earch-Moon spectrometer effect are analyzed which are geomagnetic field model, primary cosmic ray composition and hadronic interaction models. A small dataset with QGSJET-II-4 [20] + GHEISHA [21] interaction models has been generated. The expected displacement of the moon shadow from light component in east-west direction is shown in left panel of Fig.5. Comparing with EPOS-LHC + FLUKA models,

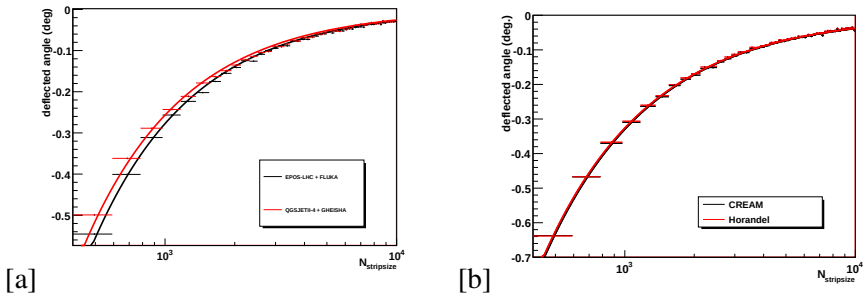

Figure 5: (a) MC west-east displacement of the moon shadow as a function of $N_{stripsize}$ from two different hadronic models. (b) is the similar result but with different primary cosmic ray composition assumption.

similar fitting function has been used to fit this displacement as function of the fired number of strips, the fitting brings about 8% difference in parameter P_0, which is taken as the uncertainty from the hadronic models. As to primary cosmic ray composition dependence, the so-called Poly-gonato model [22] is used. Comparing with the CREAM measurement, where the light component to full components ratio is around 65% in the region of 1-100 TeV, for Poly-gonato model the number of this ratio is around 62% in the same energy region. Right panel of Fig.5 shows two results comparison. Similar as left panel of Fig.5 one found that 1% difference was existed by fitting the distribution with similar function, here 1% is taken as the uncertainty from primary component composition. Finally as to the uncertainty contribution from geomagnetic model itself, from paper [23, 24], one know that comparing with the observed magnetic strength, the relative difference from the predicted model is less then 1%. Thus in this analysis, this contribution can be omitted. Hence, the total uncertainty is estimated to be around 8% in 3 to 50 TeV.

6. Conclusion

In summary based on the moon shadow phenomena, after selecting primary cosmic ray composition we carefully analyzed the so-called light moon shadow data. Through earth-moon spectrometer system, the energy of these data is directly linked with the number of fired strips due to geomagnetic field deflection. To further cross-check this energy estimator tuned by moon shadow data, a cosmic ray light component differential spectrum is calculated using the same light moon data from 3 TeV to 50 TeV, the comparison between other direct measurement shown the results was completely compatible, totally it brings around 8% difference on the differential spectrum using light moon data.

Acknowledgments: This work is supported in China by NSFC(10120130794), the Chinese Ministry of Science and Technology, the Chinese Academy of Sciences, the Key Laboratory of Particle Astrophysics, CAS, and in Italy by the Istituto Nazionale di Fisica Nucleare (INFN).

We also acknowledge the essential supports of W.Y. Chen, G. Yang, X.F. Yuan, C.Y. Zhao, R.Assiro, B.Biondo, S.Bricola, F.Budano, A.Corvaglia, B.DâĂŹAquino, R.Esposito, A.Innocente, A.Mangano, E.Pastori, C.Pinto, E.Reali, F.Taurino and A.Zerbini, in the installation, debugging and maintenance of the detector.

References

[1] B. Bartoli *et al*., ARGO-YBJ Collaboration,*Phys. Rev. D***91**, 112017 (2015)

[2] G.W. Clark, *Phys. Rev. D* **108**, (1957) 450.

[3] M. Amenomori *et al*., AS-Gamma Collaboration,*Astropart. Phys.* **28**, 137 (2007).

[4] M. G. Aartsen, *et al*., ICECUBE collaboration, Physical Review D **89**, 102004 (2014).

[5] R. Caballero et al., MINOS Observation of shadowing in the Muon Flux Underground, Merida, *ICRC* (2007).

[6] G. Aielli *et al*., ARGO-YBJ Collaboration, *Physical Review D* **84** (2011) 022003.

[7] Panov, A. D., et al., *Bull. Russ. Acad. Sci. Phys.* **73**, (2009) 564.

[8] Y. S. Yoon et al., *ApJ* **728**, (2011) 122.

[9] H. S. Ahn et al., *ApJ* **707**, (2009) 593.

[10] O. Adriani et al., *Science* **1199172**, (2011).

[11] G. Aielli *et al*., ARGO-YBJ Collaboration, *NIM* **A 562** (2006) 92.

[12] A. Aloisio *et al*., ARGO-YBJ Collaboration, *IEEE transaction on Nuclear Science* **51** (2004) 1835.

[13] C.C. Ginlay, S. Maus, C.D. Beggan, International geomagnetic reference field: the eleventh generation, *Geophys. J Int* **183** (2010) 1216.

[14] D. Heck, J. Knapp, J. Capdevielle, G. Schata, and T. Thouw, "CORSIKA: A Monte Carlo code to simulate extensive air showers", Report FZKA 6019 (1998).

[15] G. Battistoni *et al*. AIP conference proceedings **896**, 31 (2007).

[16] T. Pierog *et al*. *arXiv:1306.0121[hep-ph]* (2013).

[17] Guo Yi-Qing, *et al*., *CPC(HEP & NP)* **34**, (2010) 555.

[18] Min Zha, *Nuclear Physics B (Proc. Suppl.* **175-176**, (2008) 443.

[19] R. Fleysher, L. Fleysher, P. and A.I. Mincer, *ApJ* **603**, (2004) 355.

[20] S.S. Ostapchenko, *Phys. Rev.* **D83**, 014018 (2011).

[21] H. Fesefeldt, Report **PITHA-85/02** (1985); RWTH Aachen, available from: http:://cds.cern.ch/record/162911/files/CM-P00055931.pdf.

[22] Jorg R. Horandel *Astroparticle Physics* **19**, (2003) 193.

[23] Arnaud Chulliat and Erwan Thebault *Earth Planets Space,* **62**, (2010) 805

[24] Liu Yuanyuan *et al*. *ACTA Seismologica Sinica* **35**, (2013) 125.